SEM and TEM CHARACTERIZATION OF U-7MO IRRADIATED TO HIGH FISSION DENSITY AT RELATIVELLY HIGH POWER, HIGH TEMPERATURE, AND HIGH FISSION RATE

D. D. KEISER, JR., J. JUE, B. MILLER, A. B. ROBINSON, J. GAN, W. WILLIAMS, P. MEDVEDEV, AND D. WACHS

Nuclear Fuels and Materials Division, Idaho National Laboratory
P. O. Box 1625, Idaho Falls, ID 83415-6188 U.S.A.

Corresponding Author Contact Information:
Dennis D. Keiser, Jr.
Idaho National Laboratory
P.O. Box 1625
Idaho Falls, ID, 83415-6146 U.S.A.
Phone: 1 (208) 533-7298
Fax: 1 (208) 533-7863
E-mail: dennis.keiser@inl.gov

SEM and TEM CHARACTERIZATION OF U-7MO IRRADIATED TO HIGH FISSION DENSITY AT RELATIVELLY HIGH POWER, HIGH TEMPERATURE, AND HIGH FISSION RATE

D. D. KEISER, JR., J. JUE, B. MILLER, A. B. ROBINSON, J. GAN, W. WILLIAMS, P. MEDVEDEV, AND D. WACHS

Nuclear Fuels and Materials Division, Idaho National Laboratory
P. O. Box 1625, Idaho Falls, Idaho 83403 USA

ABSTRACT

This paper investigates the extent that irradiation conditions may impact the microstructural evolution of U-7Mo up to high fission density. This includes the effects of temperature, fission rate, and power. For a fuel irradiated in a reactor where the power, temperature, and fission rate will all be relatively high (e.g., the BR-2 reactor), it is of interest to determine if the U-7Mo responds uniquely to these conditions, compared to other reactors where the temperature, fission rate, and power are not as aggressive. In order to gain insight about the microstructural response of U-7Mo irradiated at relatively aggressive conditions, U-7Mo samples were generated from one of the most aggressively-irradiated fuel plates ever irradiated in ATR (R9R010) and characterized using scanning electron microscopy (SEM) and transmission electron microscopy (TEM). A dual-beam SEM with a focused ion beam was employed for generating samples with little surface damage. R9R010 was irradiated as part of the RERTR-8 experiment at high temperature, high fission rate, and high power, up to high fission density, and the conditions were similar to those used for the EFUTURE and SELENIUM experiments that were irradiated in BR-2. This paper will describe the as-irradiated U-7Mo microstructure for R9R010; will investigate the effects of fission rate on the microstuructural evolution of U-7Mo by comparing the observed R9R010 microstructure to what was observed for RERTR-7 fuel plates irradiated to similar fission density but at lower power, fission rate and temperature; and will discuss the potential for interconnection of fission gas bubbles at high fission density.

1. Introduction

The United States High Performance Research Reactor Fuel Development (USHPRRFD) program is actively developing low enriched uranium (LEU) U-Mo fuels for the world's research reactors that are currently fueled by uranium enriched to more than 20% ^{235}U [1]. To support development of LEU U-Mo fuels, it is important to understand how different irradiation parameters affect the microstructural evolution of U-Mo alloys. These parameters include fission density, fission rate, power, and temperature. In the BR-2 reactor, the irradiation conditions are very aggressive, and recently the SELENIUM experiment was conducted to investigate the performance of U-7Mo dispersion fuels where Si or ZrN coatings were present around the U-7Mo fuel particles. It was observed that the swelling of the fuel plates increased at high fission density (~4.5x10^{21} f/cm^3), which indicated the possible early signs of breakaway swelling [2]. Different hypotheses have been developed as to why the change in swelling was observed, including the concept that a change had occurred in the behavior of the U-7Mo fuel at high fission density.

To improve understanding of the microstructural response of U-7Mo when irradiated at high temperature, high power, and high fission rate to high fission density, a fuel plate that was one

of the most aggressively-irradiated U-Mo fuel plates ever irradiated in ATR (R9R010) was characerized using scanning electron microscopy (SEM) with energy dispersive and wavelength dispersive spectroscopy (EDS/WDS), along with transmission electron microscopy (TEM). A focused ion beam was employed to produce samples with little surface damage. To investigate the effects of fission rate on microstructural evolution on U-7Mo alloy during irradiation, comparison were made to the microstructure of other irradiated U-7Mo fuel plates that were irradiated to a similar fission density, but at lower fission rates. Evidence of interconnected porosity, which could serve as pathways for fission gas release, was also investigated.

2. Experimental
2.1 Irradiation Testing

The RERTR-8 experiment was conducted to test 6 gU/cc U-Mo dispersion fuels using enriched uranium (58.2% U-235) to control the power density of the fuel [3]. The fuel plates were positioned edge-on to the core, and as a result had a neutron flux gradient across the widths of the fuel plates. The R9R010 fuel plate was tested in the RERTR-8 experiment, and it was comprised of U-7Mo fuel particles in a pure Mg matrix and came out of the reactor in March of 2006 after 90 effective full power days of irradiation. The irradiation conditions at low and high fission density locations of the fuel plate are enumerated in Table 1. Table 2 shows the irradiation conditions for R3R050, R2R040, and R0R010 fuel plates from the RERTR-7 experiment. These are fuel plates that were irradiated to a similar fission density as R9R010 but at lower fission rates, and will be compared to in order to investigate the effects of fission rate.

Table 1. Irradiation conditions at high flux locations for fuel plate R9R010 (U-7Mo/Mg), which was tested in the RERTR-8 experiment. The temperature is increased at EOL due to growth of an oxide layer on the AA6061 cladding during irradiation.

Sample	Heat flux, W/cm^2		Temperature, ^{o}C		Fission Density, fissions/cm^3	Average fission rate density (in fuel particle), fissions/cm^3-s
	BOL*	EOL**	BOL	EOL		
R9R010 (High)	405.5	359.4	145.2	171.3	5.5 x 10^{21}	11.0 x 10^{14}
R9R010 (Low)	273.9	246.3	118.8	126.5	3.7 x 10^{21}	7.4 x 10^{14}

*Beginning-of-Life; **End-of-Life.

Table 2: Calculated irradiation parameters for R3R050, R0R010, and R2R040 SEM samples

Sample	Heat flux, W/cm^2		Temperature, ^{o}C		Fission Density, fissions/cm^3	Average fission rate density, fissions/cm^3-s	Matrix
	BOL*	EOL**	BOL	EOL			
R3R050 (High flux)	267	227	124	136	5.2 x 10^{21}	6.6 x10^{14}	AA4043***
R0R010 (High flux)	282	245	119	125	5.6 x 10^{21}	7.2 x 10^{14}	Al
R2R040 (High flux)	337	307	121	119	6.3 x 10^{21}	8.1 x 10^{14}	Al-2Si

*Beginning-of-Life; **End-of-Life; ***Nominal composition (wt.%): (4.53Si-0.14Fe-0.09Cu-0.04Ti-0.01Zn-0.008Mg-balAl)

2.3   Microstructural Characterization

At the Hot Fuels Examination Facility (HFEF) at the Idaho National Laboratory, a thin slice (~ 1-mm-thick) was produced from the low and high-fission density side of the R9R010 fuel plate using a slow-speed saw. The samples were then transferred to the Electron Microscopy Laboratory where they were mounted and polished and inserted into a scanning electron microscope (SEM). Both secondary electron (SE) and backscattered electron (BSE) images were produced from the polished samples. Additional characterization samples were produced from the mounted samples using a FEI Quanta3D Dualbeam focused ion beam (FIB). Mulitple "lift-outs" were produced at specific locations by coarse trenching approximately a 20 μm x10 μm x 1 μm sample so that surfaces with little polishing damage could be obtained. SE imaging was employed to evaluate the the size, morphology, and distribution of fission gas bubbles and solid fission product phases present in these samples. In addiiton, FIB was employed to produce samples for transmisison electron microscopy (TEM) analysis. To produce information for 3D reconstruction, two cubes, each with dimensions of ~(20 μm x 20 μm x 25 μm), were produced from the U-7Mo. Tens of nanometers of material was milled at a time from the cube, and an SEM image was produced after each milling step. The hundreds of images that were generated were used in combination with a software program to produce 3D reconstruction information.

3.   Results

3.1   Scanning Electron Microscopy

3.1.1 Low-Flux Sample

Due to the fact that negligible fuel matrix interaction is observed for a disperion fuel plate with Mg matrix [3], one does not need to avoid a fuel/matrix interaction (FMI) layer when characterizing U-7Mo fuel particles. The microstructure of a FMI layer can be quite different than irradiated U-7Mo and can complicate the characterization process [4]. Fig. 1 shows an SE image of the fuel particles observed in the center of the R9R010 fuel meat for a polished sample, and as expected, no signs of interaction layers are apparent around the fuel particles. Fig. 1b shows the Mg-Al interaction layer present at the fuel meat/AA6061 cladding interface. This interaction zone forms during fabrication and is present during irradiation. A fractured U-7Mo fuel particle is presented in Fig. 1c showing the location of relatively large fission gas bubles on the cell boundaries of the irradiated U-7Mo. Fig. 2 shows the results of x-ray mapping for U, Mo, and Mg, which confirms the lack of fuel/matrix interaction. Figure 3 shows the microstructure for a U-7Mo fuel particle located at the fuel meat/AA6061 cladding interface. It was observed that where the fuel particle was in contact with the AA6061 cladding, a FMI interaction layer, around 10-μm-thick, had formed during fabrication and/or irradiation. The interaction layer at this location had a composition, in at.%, of 15U-4Mo-79Al. Moving from the AA6061 cladding towards the center of the fuel meat, the Mg/AA6061 interaction zone was observed to become more enriched in Mg. The fuel/matrix interaction layer around the U-7Mo fuel particle became thinner as the interaction zone became more enriched in Mg. There was a negligible FMI layer formation once the Mg-Al matrix reached a composition of around 51Mg-48Al (at.%). Based on the Mg-Al phase diagram, this is near the composition of a $Mg_{17}Al_{12}$ phase [5].
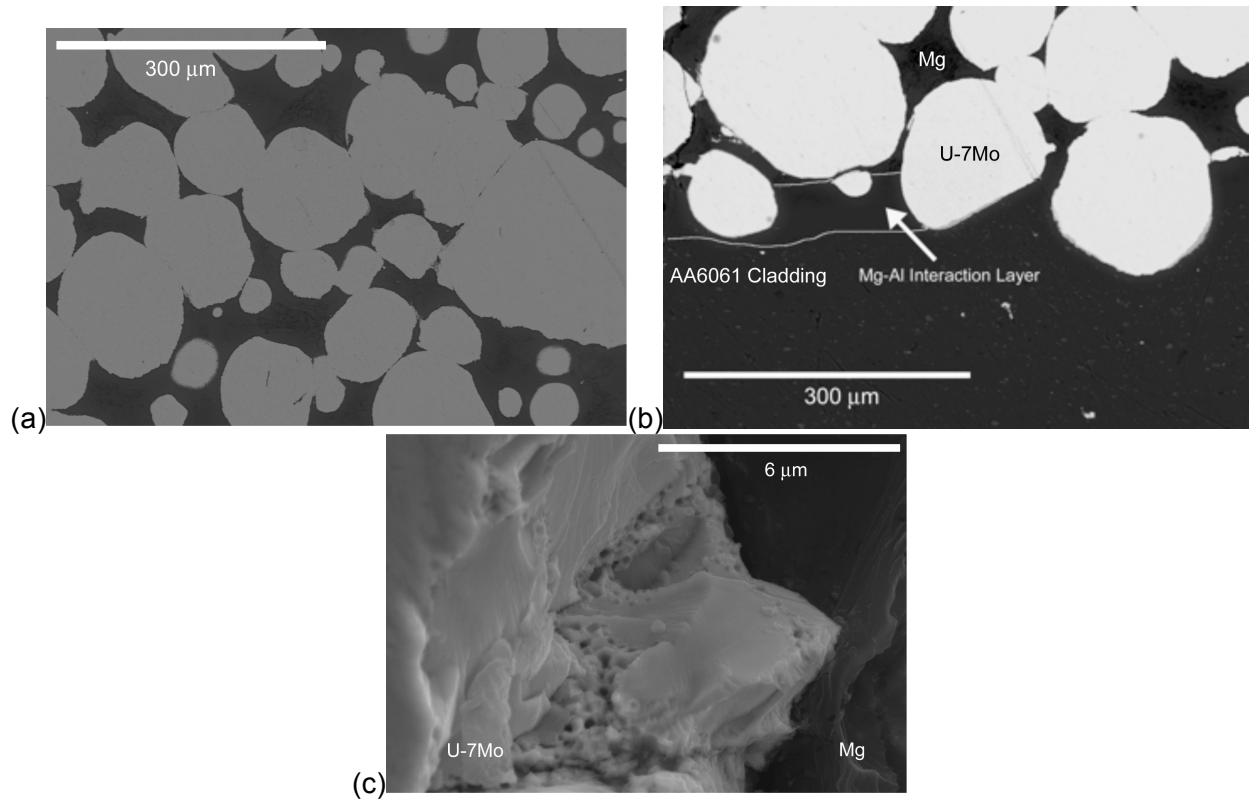
Fig. 1. For the low-flux R9R010 sample, (a) is a BSE image of the polished surface of the sample at the center of the fuel meat, (b) is a BSE image near the fuel meat/AA6061 cladding interface, and (c) is an image of a fracture surface observed for one of the fuel particles. The lines in (b) identify the thickness of a Mg-Al interaction layer.
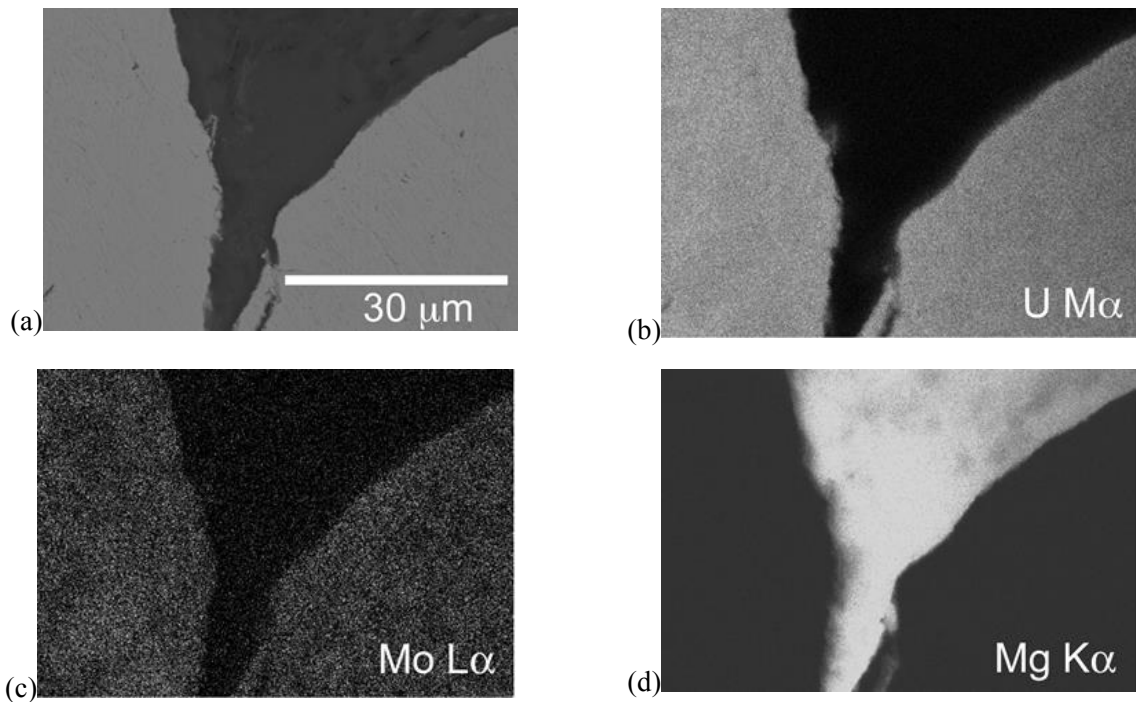
Fig. 2. (a) BSE image for the R9R010 low-flux sample, and x-ray maps for (b) U, (c) Mo, and (d) Mg.
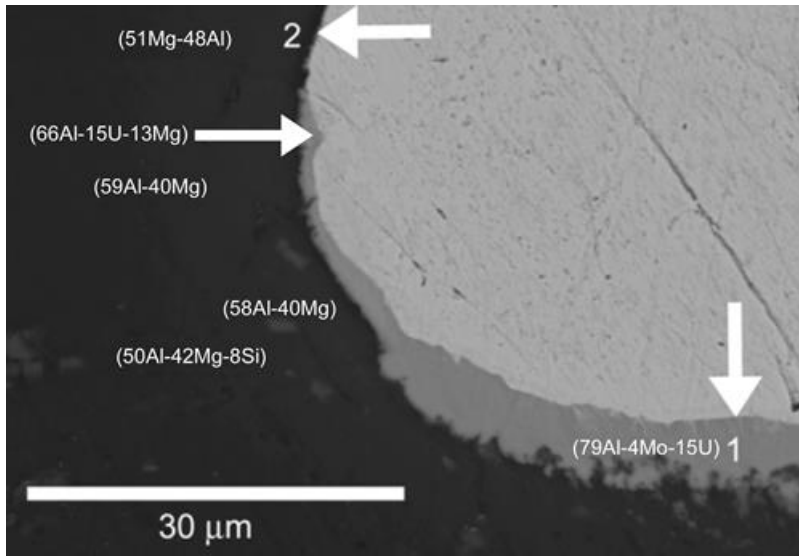
Fig. 3. BSE image for the low-flux sample showing a fuel particle near the fuel meat/AA6061 cladding interface, and the measured compositions at specific locations (at.%) in the Mg-Al interaction layer. Nearest the cladding where more Al is present in the Mg-Al interaction layer, a relatively thick interaction layer is present. The thickest layer that contains U, Mo, and Al is present at the U-7Mo/cladding interface (point 1). The fuel/matrix interaction layer becomes negligible (point 2), where the Mg-Al interaction layer contains around 51 at.% Mg.

To determine the variability of the Mo concentration through a U-7Mo fuel particle after irradiation, a compositional EDS linescan was produced (see Fig. 4c). The Mo content mean was observed to be 7.2 wt.%, the standard deviation was 1.1, the maximum Mo concentration was 9.4 wt.%, and the minimum Mo concentration was 5.1 wt.%. The variation in Xe concentration was also plotted (Fig. 4c), and the maximum Xe was measured to be around 1.0 wt.%. The Xe is released (approaches zero in concentration) from the material in the cell boundary locations when the larger bubbles are penetrated during sample preparation, but it is retained in the material (approaches 1 wt.%) away from the cell boundaries, where the Xe is contained in a fission gas superlattice [6]. SEM images of FIB-produced samples are presented in Fig. 5, and these images show the relatively large fission gas bubbles present around cell boundaries. In some areas, the large bubbles are almost present throughout the microstructure of the sample (see Fig. 5b).

(a)

(b)

(c)
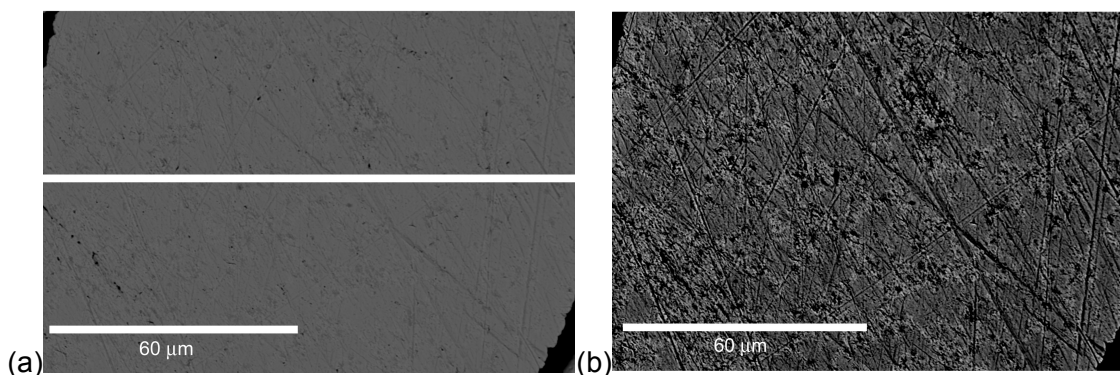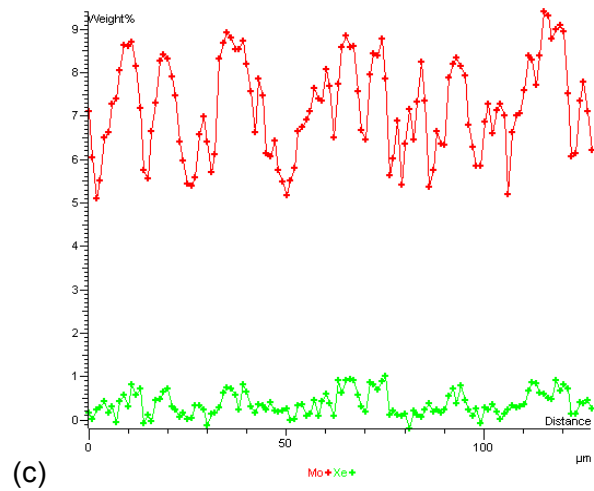
Fig 4. For the low-flux sample, (a) a BSE image showing a line along which compositional analysis was performed, and (b) a BSE image with contrast/brightness adjustment to highlight the large fission gas bubbles on cell boundaries with low Mo content. (c) is a compositional scan along the line in (a) where the results for Mo (red) and Xe (green) are plotted.
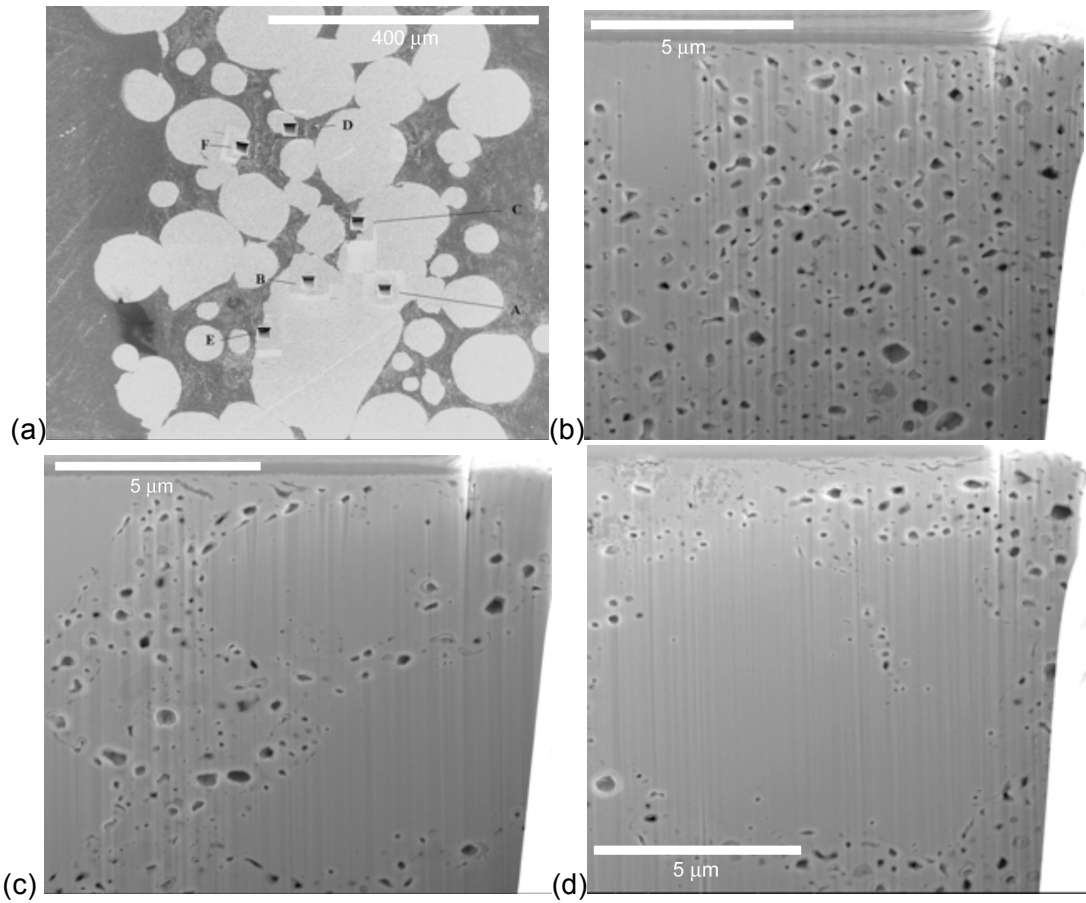
Fig. 5. (a) BSE image showing where FIB samples were produced from the polished surface of the low-flux R9R010 sample. (b-d) show example BSE images (12KX) of the FIB samples taken from the locations A-E in Figure 5(a).

3.1.2 High-Flux Sample

Fig. 6a shows a BSE image of the fuel particles observed in the center of the high-flux R9R010 fuel meat for a polished sample. In Fig. 6b, a relatively high magnification image is presented, and no U-7Mo/Mg interaction zone is apparent. Like was the case for the low-flux sample, a U-7Mo fuel particle that was in contact with the AA6061 cladding developed an interaction layer (see Fig. 6c), and this layer was not present when the fuel particle was in contact with Mg-enriched Mg-Al matrix. X-ray maps for U, Mo, Mg, and Xe are presented in Fig. 7. During irradiation, no interaction of U and Mg is observed. The fracture surfaces observed for three different fuel particles are presented in Fig. 8. Only relatively large fission gas bubbles are observed. EDS linescans were generated to determine the variability of the Mo, Xe, and Nd for different fuel particles. Fig. 9 shows the results for one fuel particle, and it can be seen that there is variability in the concentrations for these constituents.   For Mo, the mean concentration was 7.5 wt%, the standard deviation was 1.0, the maximum Mo concentration was 9.2 wt%, and the minimum Mo concentration was 5.2 wt%.
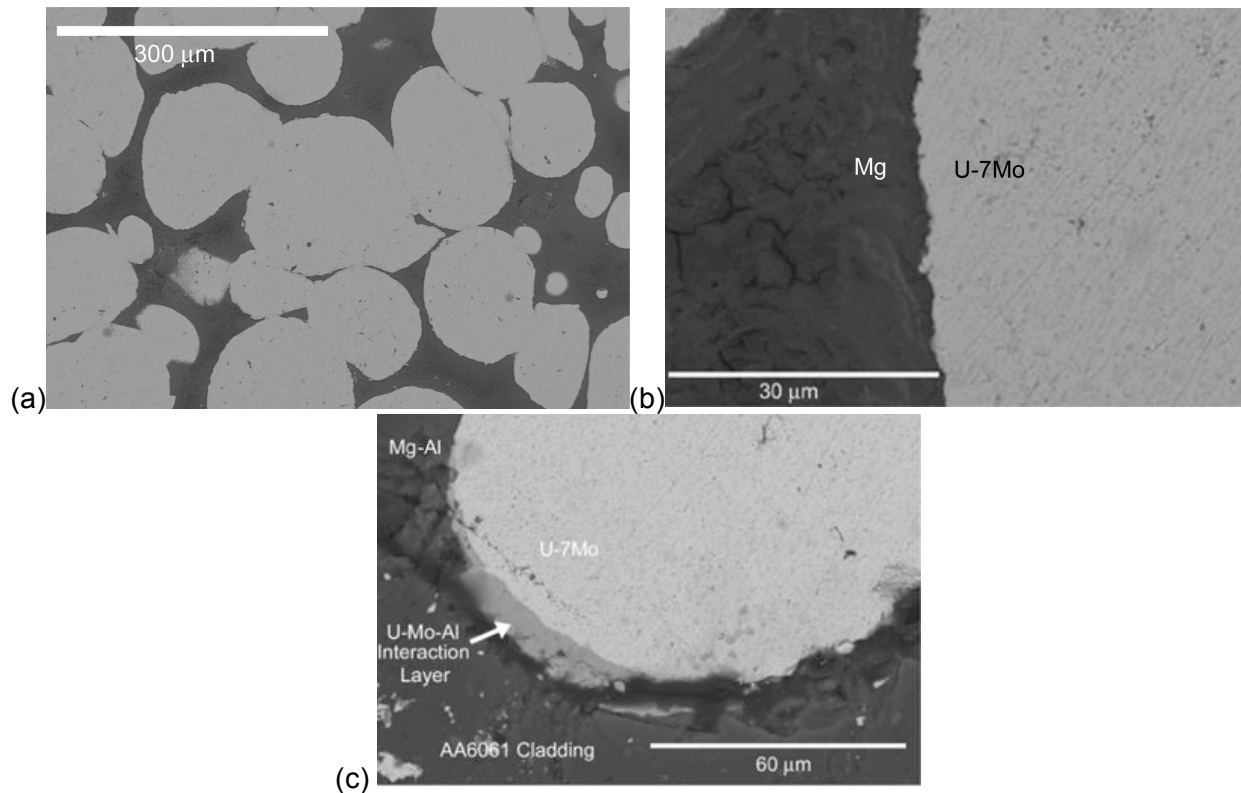
Fig. 6. For the high-flux R9R010 sample, (a) and (b) are BSE images of the polished surface of the sample, and (c) is a BSE image showing a U-7Mo particle in contact with the AA6061 cladding, the interaction layer that has formed at the interface with the cladding, and the lack of interaction layer where there is contact with a Mg-rich, Mg-Al phase.
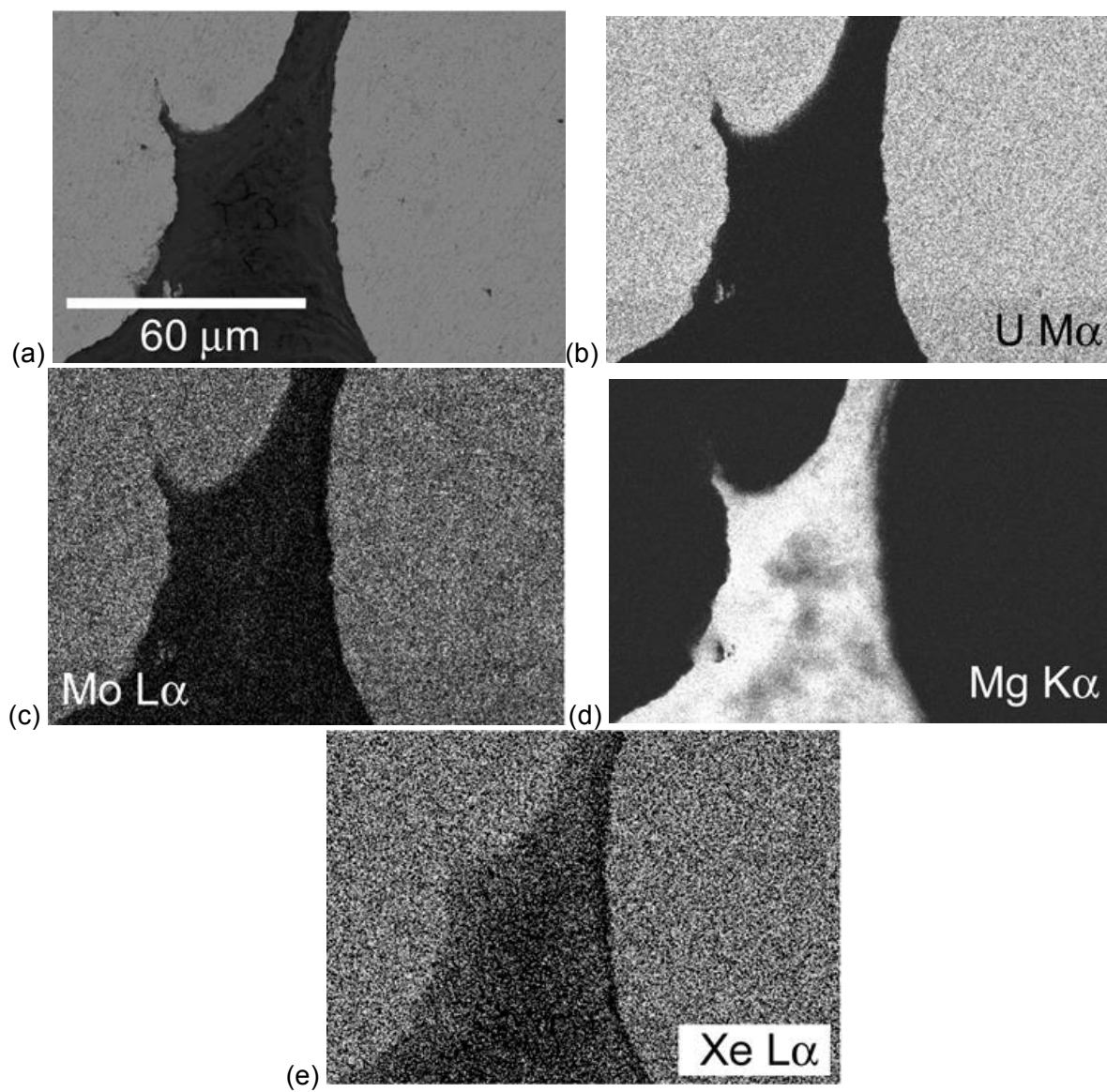
Fig. 7. BSE image (a) and x-ray maps for (b) U, (c) Mo, (d) Mg, and (e) Xe.

(c)
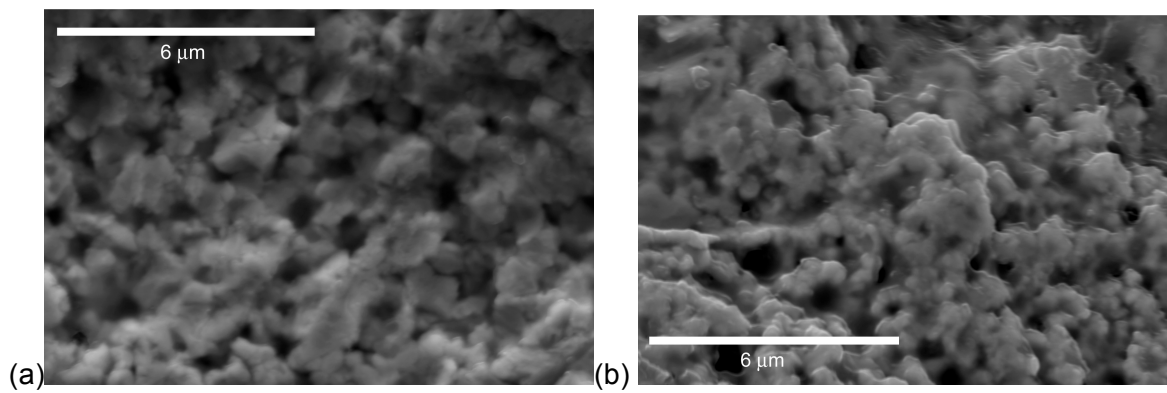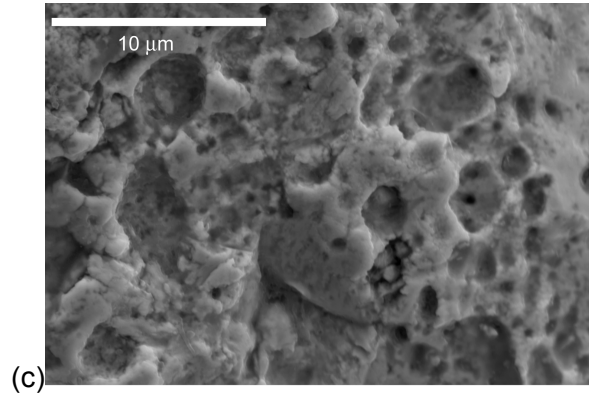
Fig. 8. For the high-flux R9R010 sample, (a-c) are SE images of the fracture surfaces observed for three different fuel particles.

(a)

(b)
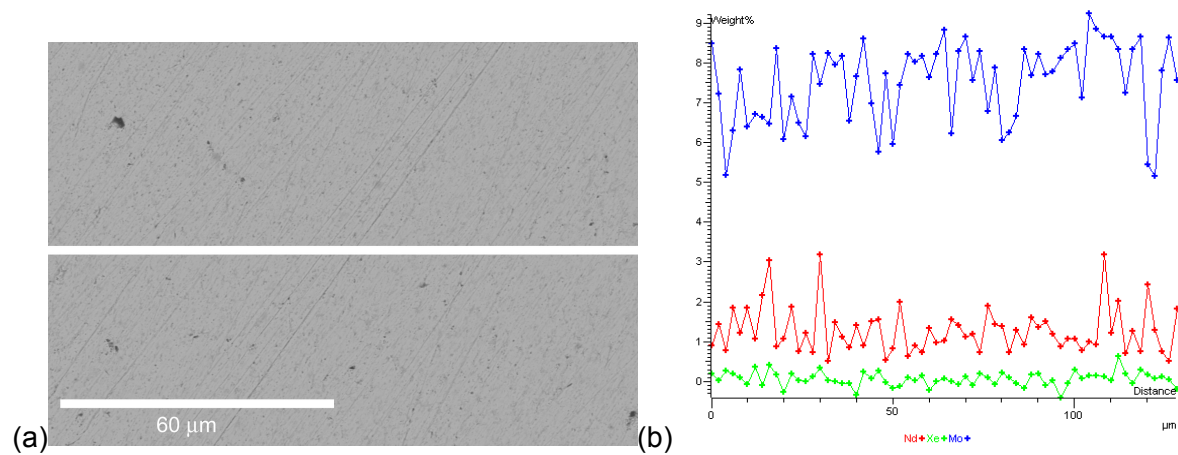
Fig 9. BSE image (a) showing a line along which compositional analysis was performed. (b) shows a plot of the results for Mo (blue), Xe (green), and Nd (red).

Fig. 10 presents SEM images of three different FIB samples selected from the surface of the polished sample (Figure. 10a) to reveal the microstructure of U-7Mo at high fission density. No residual fuel grain areas (areas that only contain fission gas superlattice bubbles) are observed, like were seen in the low-flux sample. Higher magnification images are presented in Figure 11 that show regions in some fuel particles where fission gas bubble interconnection seems to be apparent, and in many cases "pathways" are present that connect directly to the U-7Mo/Mg interface. These features are unique to the R9R010 sample, and have not be seen other lower fission rate samples that have been characterized using the same techniques, up to this point in time. As shown in Fig. 11e, solid fission product phases can be found that are located at the U-7Mo/Mg interface. Using higher magnification SEM images, it is possible to reveal finer-scale features in the U-7Mo that was irradiated in the R9R010 fuel plate. As shown in Fig. 12, the U-7Mo grains are a few hundred nanometers in size, and grain boundary "triple points" can be resolved where porosity is present, which in some cases seems to contain solid fission products. When looking at the larger fission gas bubbles in the microstructure, it is apparent that grain boundaries are in most cases associated with these bubbles, due to all the fine grains that comprise the microstructure. Interestingly, some fuel particles (see Fig. 13) have been identified that do not contain the "pathways" to the U-7Mo/Mg interface shown in Fig. 11. Instead, at the U-7Mo/Mg interface areas are present without observable fission gas bubbles (suggesting the presence of the fission gas superlattice where a TEM would be needed to see the fission gas bubbles). This variation in observations at the U-7Mo/Mg interface could be due

to differences in the quality of contact at the interface. For cases where bonding is good, there is good heat transfer, resulting in a reduction in the temperature at the interface. This means the bubbles may remain smaller due to lower mobilities of fission gases and irradiation-produced defects. However, when the bonding at the U-7Mo/Mg interface is poor, possible due to the presence of an oxide layer, the heat transfer will not be as effective and the temperature will remain high, and so will the fission gas bubbles will remain large due to higher mobility of fission gases and irradition-produced defects that results in growth of bubbles.
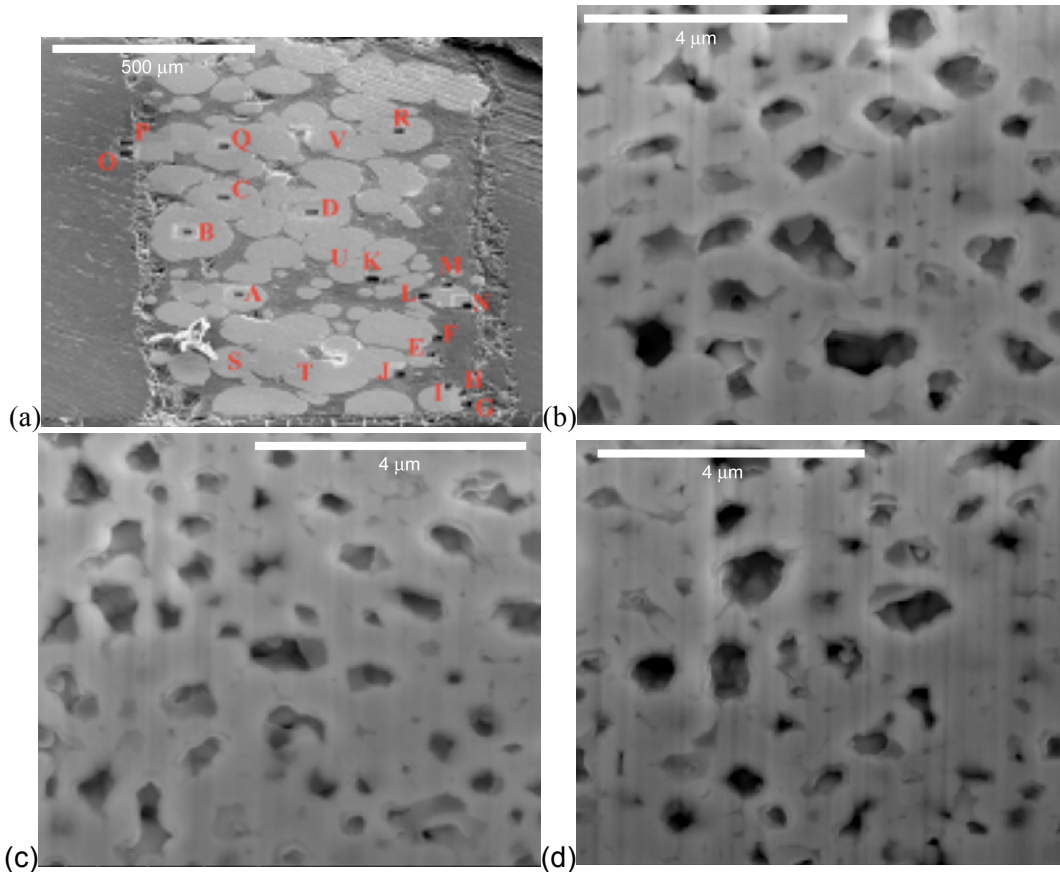
Fig. 10. SEM micrograph (a) showing locations where FIB samples were produced from the R9R010 high-flux sample. (b-d) are FIB images for samples A-C, which were generally at the center of the fuel particles.
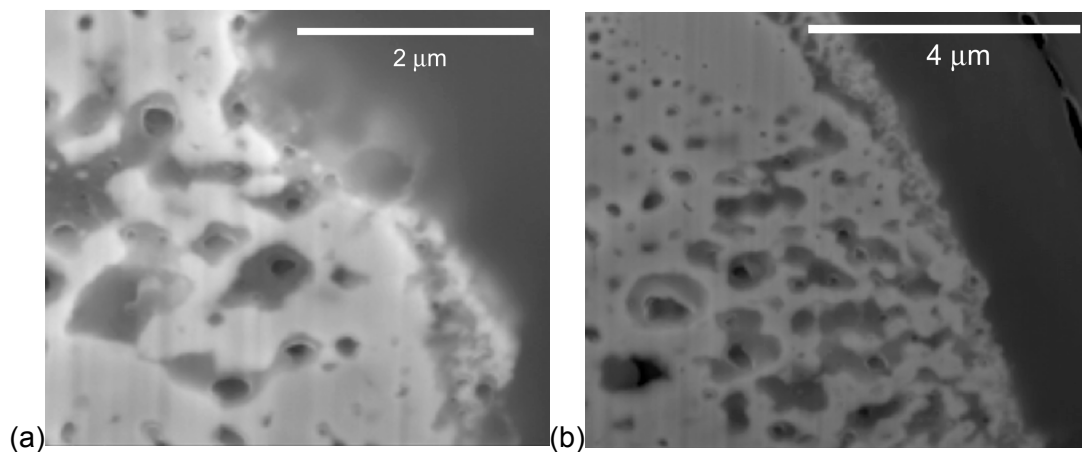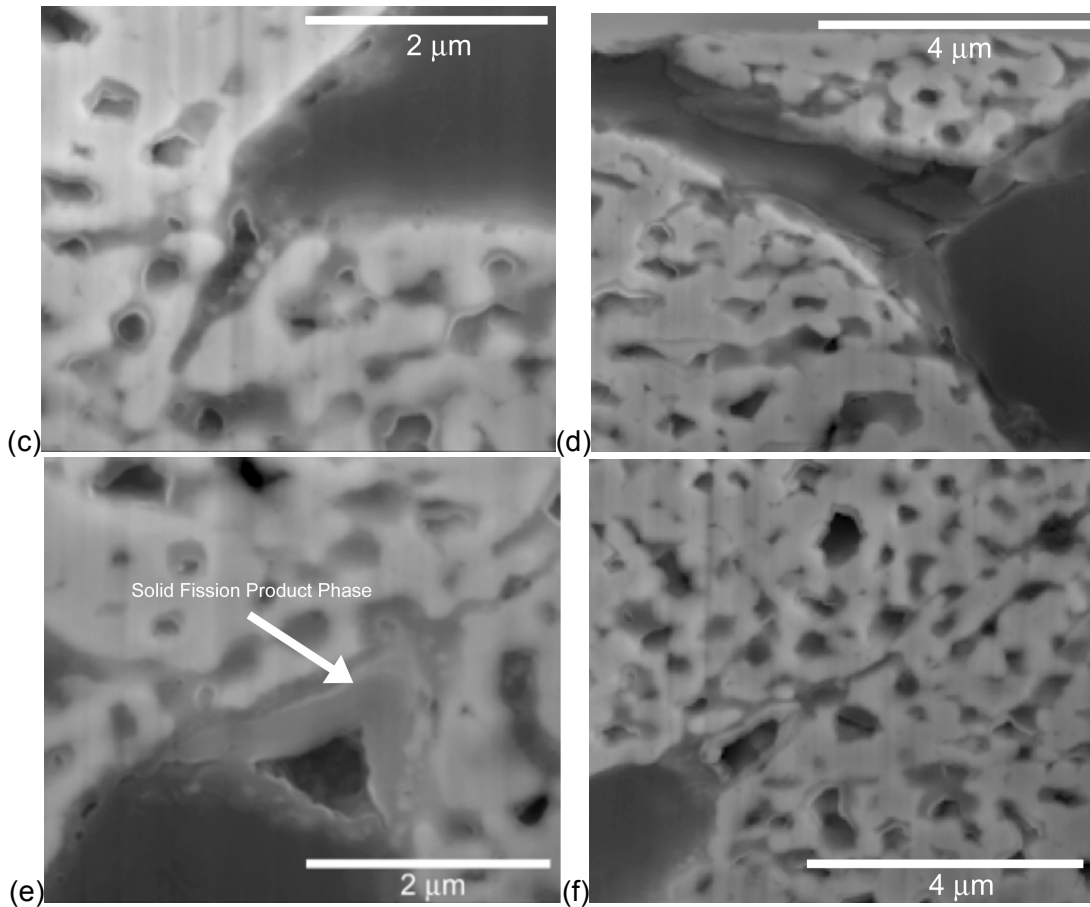
Fig. 11. SEM micrographs (a-f) from R9R010 high-flux FIB samples that show interconnection of fission gas bubbles and microstructural pathways to the U-7Mo/Mg interface.
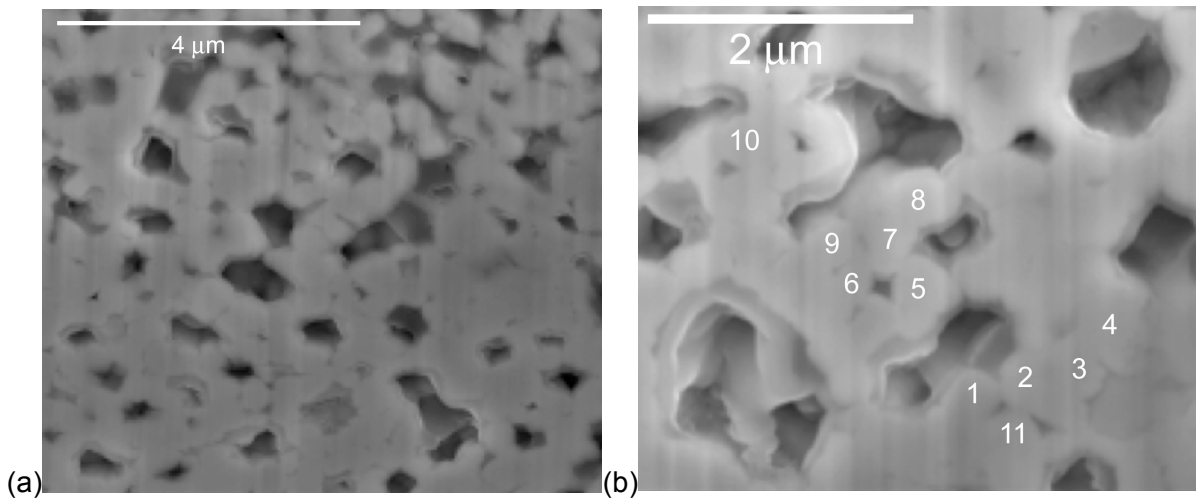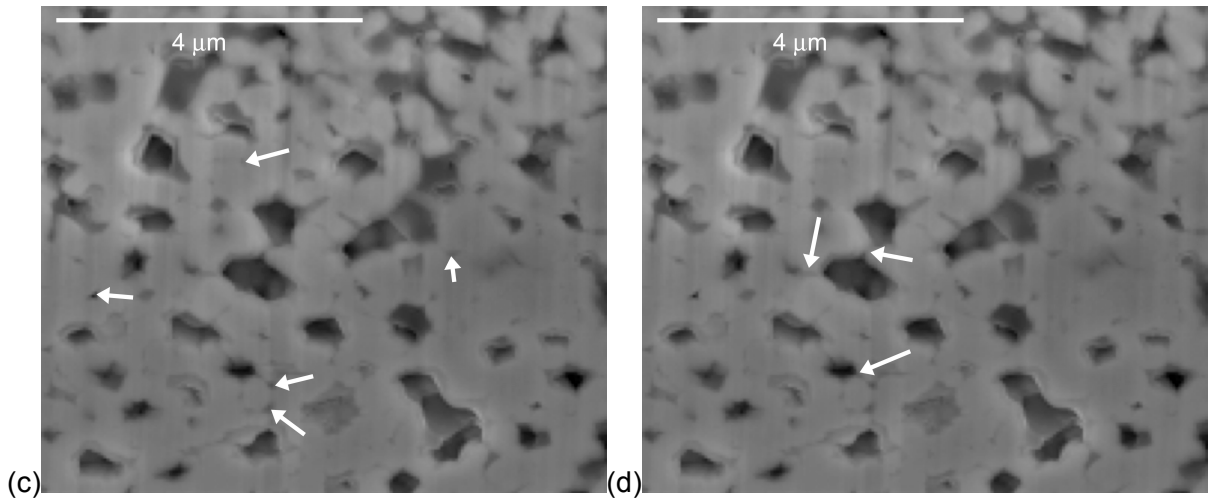
Fig. 12. SEM micrographs showing the microstructures for R9R010 FIB samples generated from different fuel particles. In (b) some of the small grains (a few hundred nanometers in size) have been numbered to highlight their size. Image (c) is the same image in (a) where grain boundary "triple points" that contain pores or solid fission products have been identified with arrows. In image (d), arrows are used in the (a) image to highlight how the large fission gas bubbles typically have grain boundaries connected to them.
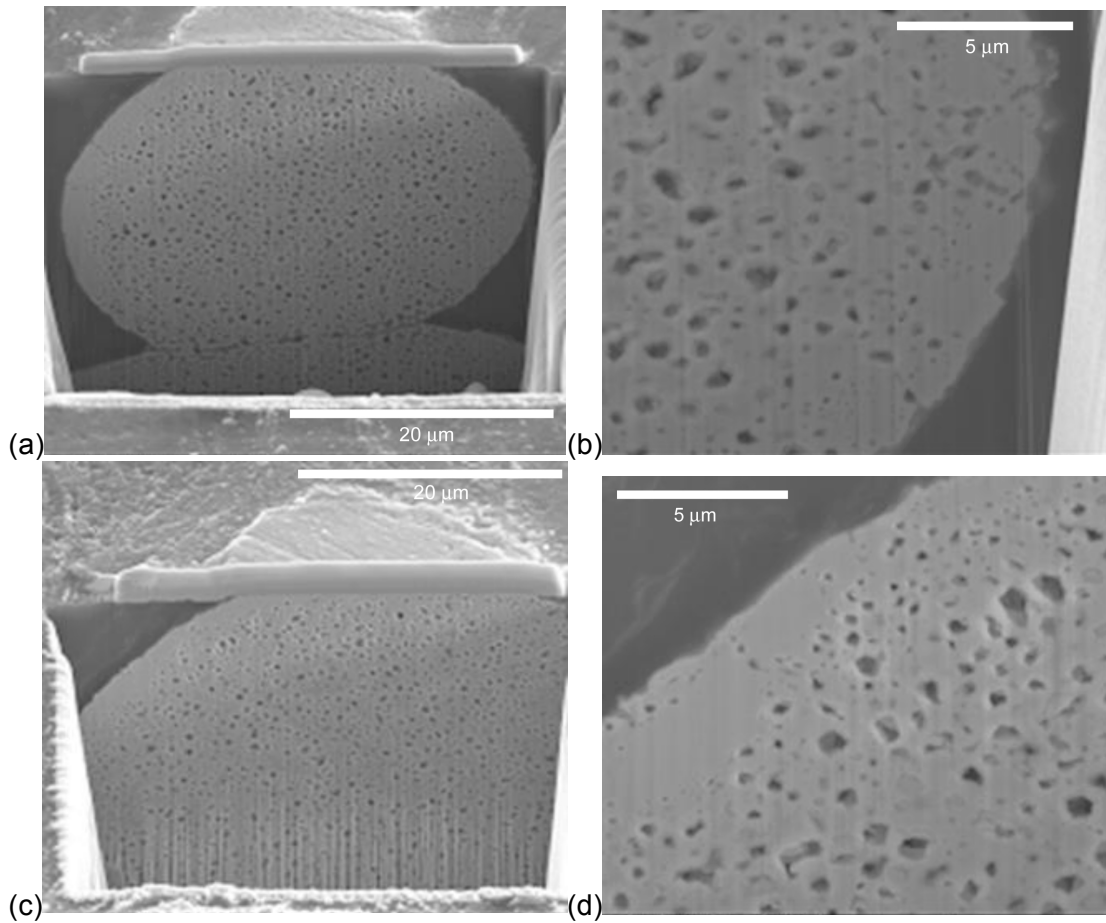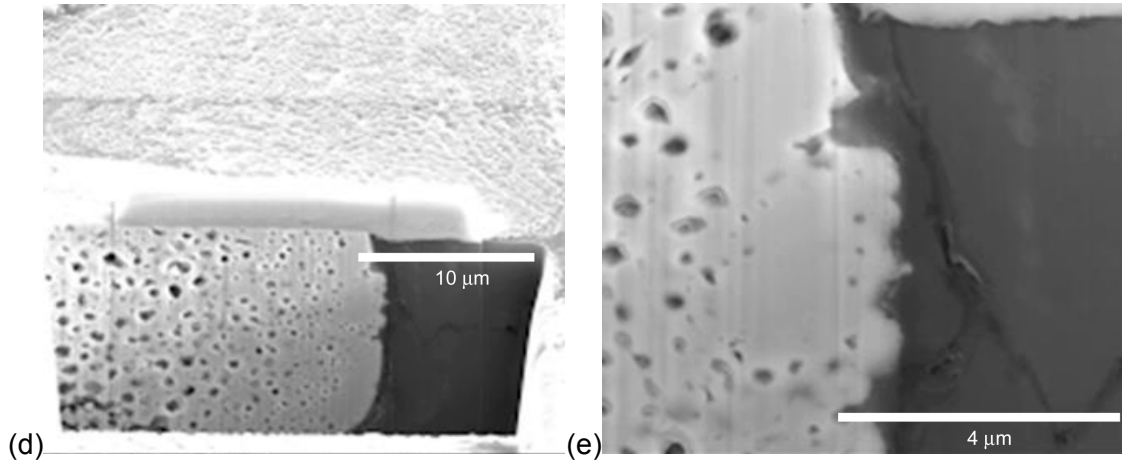
Fig. 13. BSE images (a-e) showing regions near the U-7Mo/Mg interface where less relatively large fission gas bubbles are observed (arrows).

3.2   Transmission Electron Microscopy

TEM analysis was performed to characterize the microstructure of the fuel particles and to look for any evidence of interaction betweent the U-7Mo particles and Mg matrix. An SE image of a TEM sample being produced is presented in Fig. 14(a), along with TEM micrographs for images taken at (b) 800X, and STEM images taken at (c) 5,000X, and (d) 20,000X. These micrographs show the regions present in the microstructure with relatively fine and large fission gas bubbles, and the fact that the bubbles are typically faceted, not round. A TEM micrograph taken of the U-7Mo/Mg interface is presented in Fig. 15, and Table 3 enumerates the result for various EDS measurments taken into the Mg and U-7Mo. Negligible interaction of the U-7Mo and Mg was observed.

(c)   *(d)*
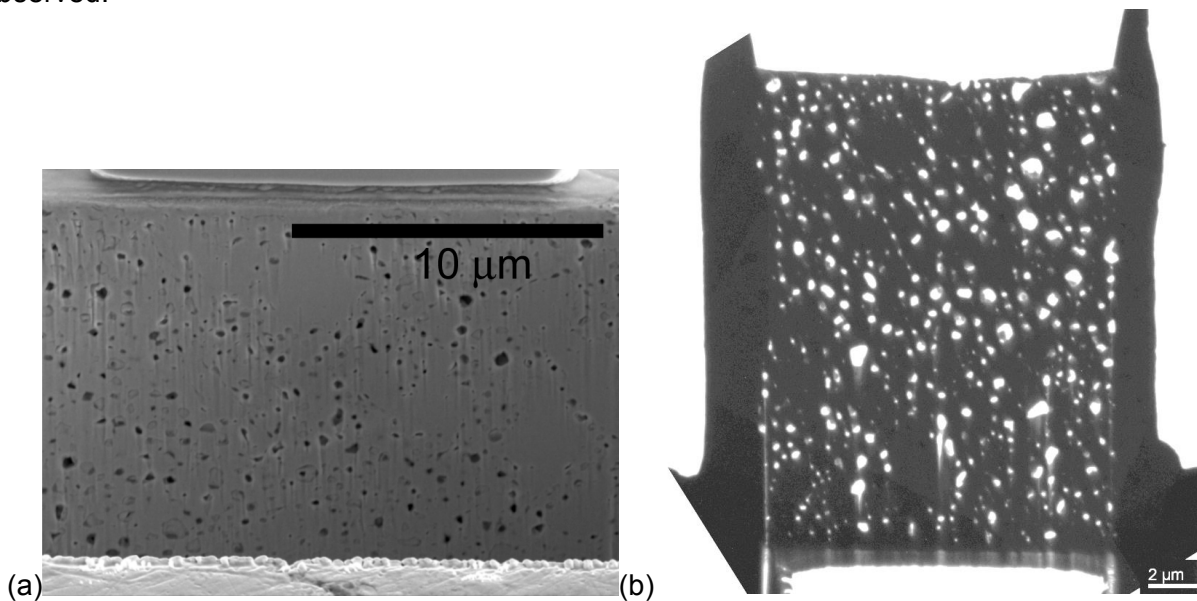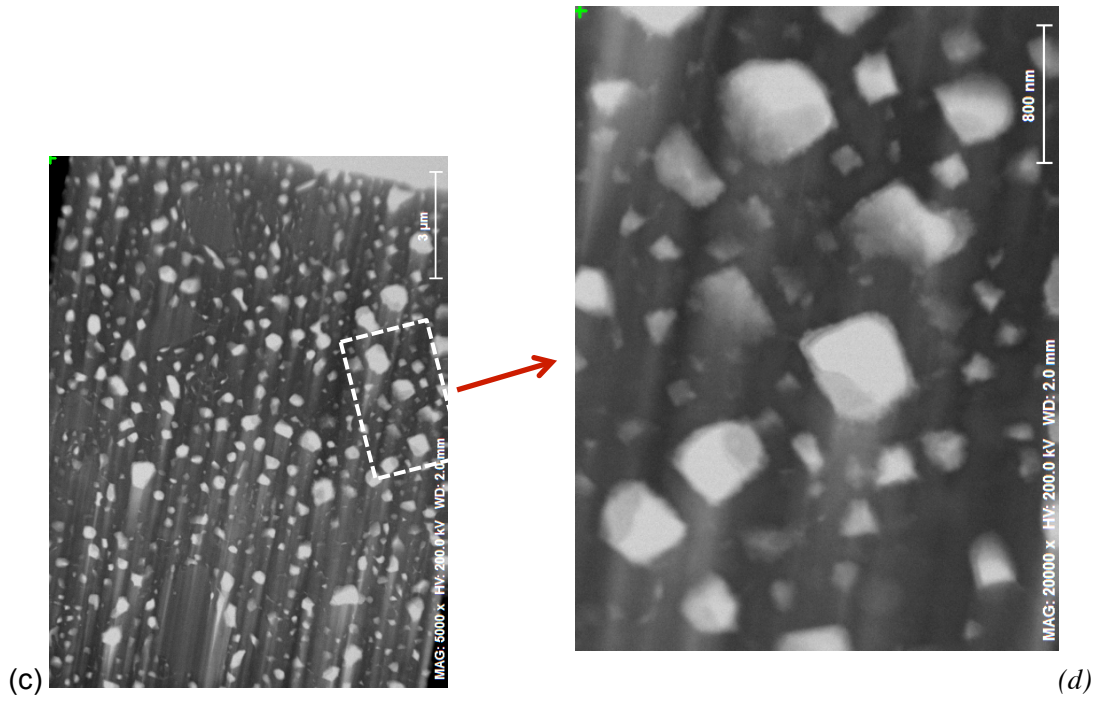
Fig. 14. SEM micrograph (a) showing TEM sample being FIBed. (b) is a montage of low magnification TEM images of the FIB sample. (c) is a scanning TEM image with an enlarged view of the boxed area shown in (d).
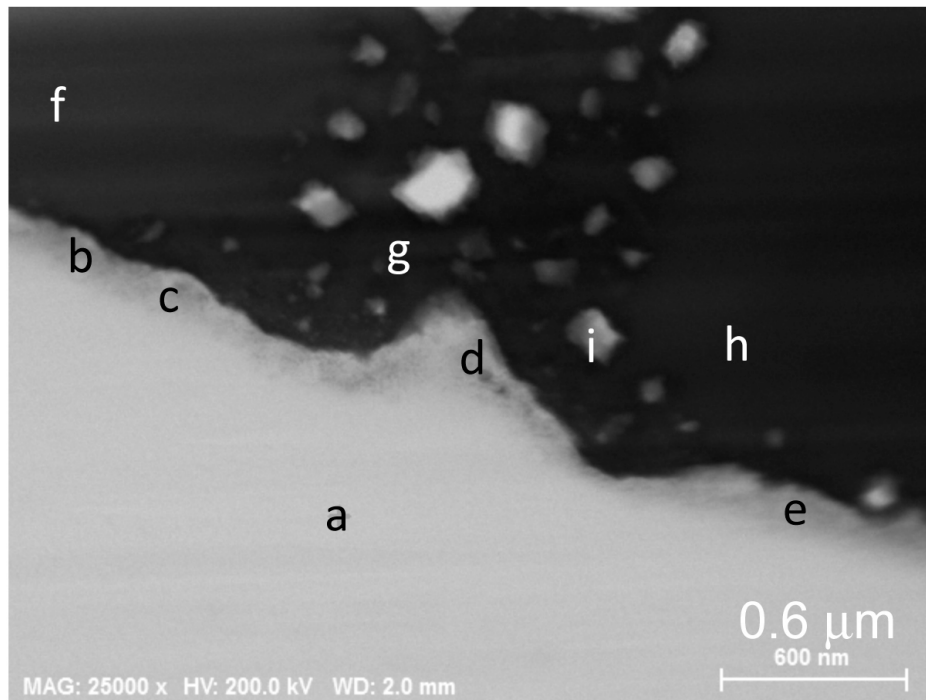
Fig. 15. TEM micrograph showing the interface for a U-7Mo fuel particle in contact with Mg matrix. The labels identify locations where EDS analysis was performed.

Table 3. Results (at.%) for compositional analysis conducted at the points identified in Fig. 15.

Spot	Mg	Oxygen	U	Mo	Comments
a	92	8	-	-	Mg matrix
b	63	5	23	10	Mg side next to fuel
c	76	13	7	3	Mg side next to fuel
d	74	8	12	6	Mg side next to fuel
e	73	7	14	6	Mg side next to fuel
f	0	4	65	31	U-Mo fuel
g	1	1	70	27	U-Mo fuel
h	0	3	67	30	U-Mo fuel
i	3	5	69	23	U-Mo fuel

3.3   3D Reconstruction

Fig. 16 shows an SE image of a cube from sample R3R050 that is used for 3D reconstruction. Figures 16 (b-d) show the reconstructions produced for samples R2R040, R3R050-1, and R3R050-2. Similar 3D reconstruction was performed on two samples produced from R9R010. Color shading is used in the reconstructions to highlight regions where bubble are becoming interconnected. Fig. 17 is a computer image showing fission gas bubbles that have become interconnected in a sample produced from the R3R050 fuel plate. The 3D reconstructions confirm that there is interlinking of bubbles within the irradiated U-7Mo fuel particles. All five samples show some interconnection of porosity.

(a)   (b)
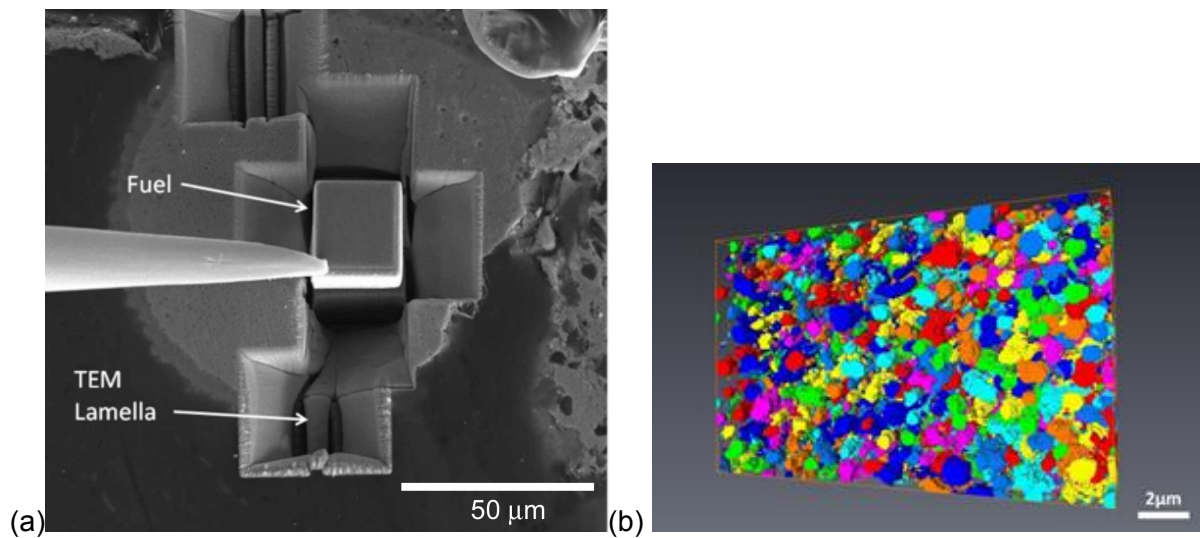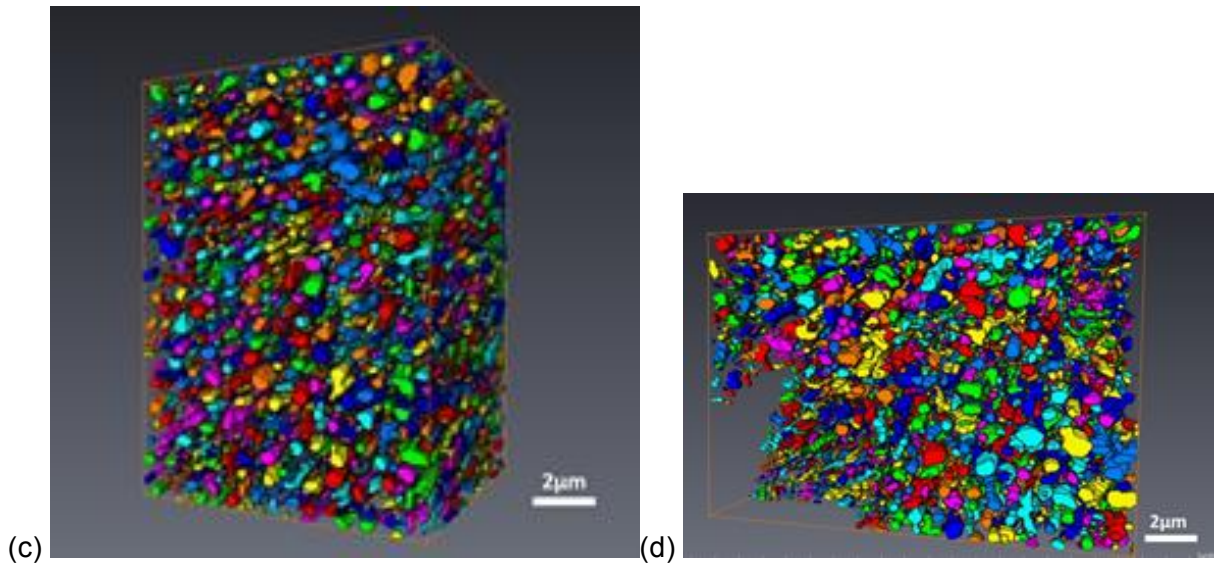
Fig. 16. (a) SE image of a cube generated from sample R3R050, and 3D reconstructions for samples (b) R2R040, (c) R3R050-1, and (d) R3R050-2. Color shading is used to highlight local regions where bubbles are becoming interconnected. (c) and (d) are for two different fuel particles contained in the R3R050 sample.
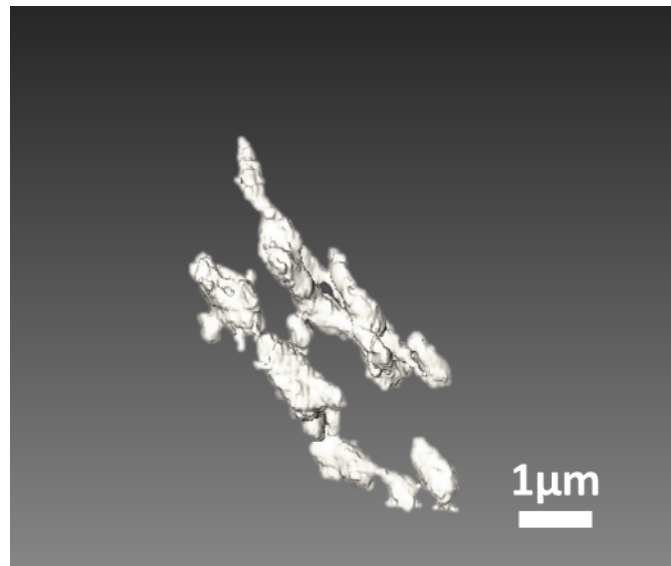
Fig. 17: Interlinking of fission gas bubbles in sample R3R050-2.

Using the Avizio software program, pore size distributions were determined for each 3D reconstruction. In samples where residual fuel grains are present (i.e., have no observable fission gas bubbles because they are contained in a fission gas superlattice), the grain is removed from the porosity calculations. Fig. 18 shows the porosity size distributions for the five samples where a 3D reconstruction was performed, including the two from R9R010. Note that the porosity distributions were normalized for comparison. Additionally, the fission densities in units of 10^{21} fissions/cm^3 are provided in the legend. Fig. 18 can be used to show how the porosity distributions vary for different fission densities. It should be remembered that the two R9R010 samples were also exposed to a higher fission rate. The plots show that, compared to

R2R040 and R3R050, the R9R010 sample microstructures contains a higher percentage of larger fission gas bubbles and a lower percentage of the small bubbles. Figure 18 also shows that the porosity size distributions for the two cubes from the R3R050 sample are different. These cubes came from two different fuel particles, and this difference could be due to a difference in Mo content between particles, such that a lower Mo content particle develops more larger bubbles at a similar fission density.
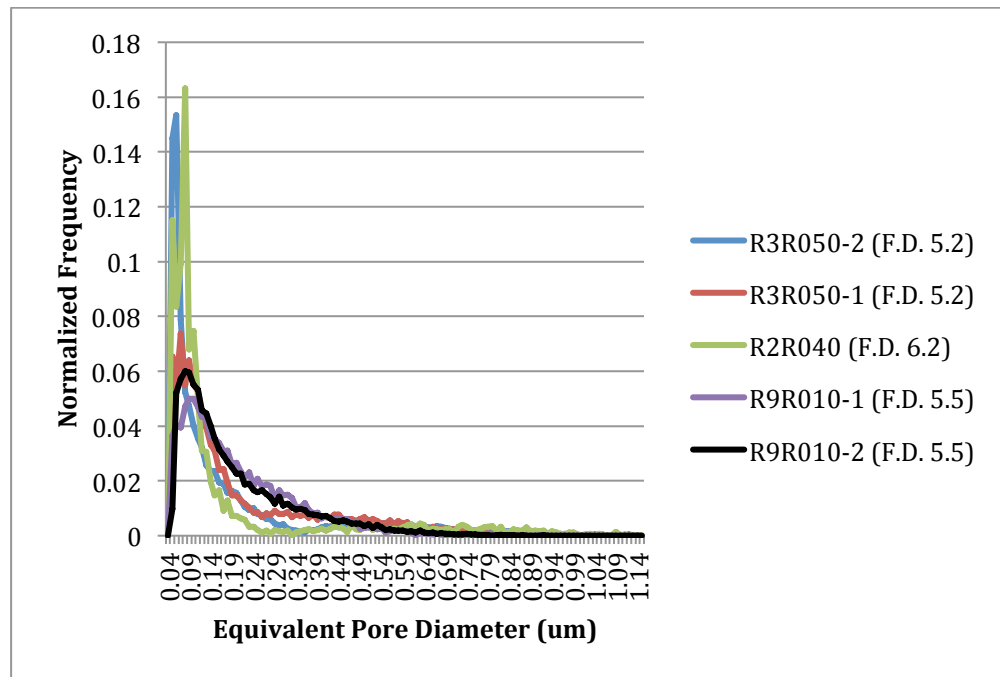
Fig. 18: Porosity size distribution for two R3R050 samples, one R2R040 sample, and two R9R010 samples.

4.   Discussion

4.1 Comparison to fuel plates irradiated under similar conditions

Based on the microstructural characterization performed on low and high-flux samples produced from R9R010, the microstructure of a Mg-matrix dispersion fuel differs from what has been reported for U-7Mo fuels with Al-Si matrices, which were irradiated in the EFUTURE experiment under similar conditions in the BR-2 reactor (see Table 6), and ZrN-coated U-7Mo dispersion fuel with Al matrix irradiated in the SELENIUM experiments, also irradiated in the BR-2 reactor (see Table 7). The SELENIUM plates achieved maximum power at beginning-of-life (BOL), and due to a lack of burnable neutron absorbers, there was a reduction in power with irradiation time. [7] The power was around 250 W/cm^2 at end-of-life. Taking into account the peak power of 466 W/cm^2, the fission rate for the SELENIUM fuel plate U7MD1231, which contained ZrN-coated U-7Mo powder, would have been very close to what was achieved for the R9R010 high flux sample. From a power perspective, the R9R010 high flux sample was at higher power at end-of-life (EOL) (359.4 W/cm^2) than were the plates irradiated in SELENIUM.

Table 6. Irradiation Conditions for EFUTURE samples [8].

Plate ID Cladding	U7MC4111 ALFENI	U7MC4202 AG3NE	U7MC6111 AlFeNi	U7MC6301 AG3NE
Fabrication data				
Si% in Al matrix	4%	4%	6%	6%
Thermal treatment	425°C-2h	475°C-2h	425°C-2h	475°C-2h
Irradiation data				
Mean Bu (%U-235)	48.3	48.1	47.1	47.5
(f/cm3 U(Mo))	3.63×10^{21}	3.62×10^{21}	3.53×10^{21}	3.57×10^{21}
Max BU (%U-235)	71.3	71.3	68.7	71.4
(f/cm3 U(Mo))	5.53×10^{21}	5.53×10^{21}	5.31×10^{21}	5.54×10^{21}
Peak heat flux (Wcm-2)	457	453	465	472

Table 7. Irradiation Conditions for SELENIUM samples [2].

Plate ID	U7MD1221	U7MD1231
Cladding	AG3NE	AG3NE
Matrix	Al	Al
Coating	600 nm Si	1000 nm ZrN
Loading (gU/cc)	8	8
Enrichment (% U-235)	19.75	19.75
EFPD	69	69
Mean BU (% U-235) (f/cc U(Mo))	47.9 (3.5×10^{21})	47.5 (3.5×10^{21})
Max BU (% U-235) (f/cc U(Mo))	69.2 (5.3×10^{21})	69.6 (5.3×10^{21})
Peak Heat Flux (W/cm^2)	421	466

A nice feature of Mg matrix fuel is that the different phases (U-7Mo, Mg, cladding) in the fuel plate (except for maybe a few regions in the U-7Mo fuel particles around large fission gas bubbles that can go amorphous) remain crystalline, and most importantly the U-7Mo and Mg do not interact, even when irradiated to a relatively high fission density. This is not the case for dispersion fuels with Al or Al-Si matrices, which form U-bearing interaction layers around the fuel particles that go amorphous [6]. These layers do not contain fission gases well, meaning that fission gases are mobile and either form large fission gas bubbles in the layers or at interfaces with the layers. When characterizing EFUTURE microstructures after irradiation to different fission densities, plastic flow of the interaction layer was observed, along with large fission gas bubbles that exhibited interconnection. [8] For the microstructures of ZrN-coated U-7Mo fuel particles dispersed in Al matrix (U7MD1231) after irradiation to a fission density near 5.0×10^{21} f/cm^3, there was evidence of interaction layer formation that penetrated into the U-7Mo particles, even though a ZrN coating was present around the fuel particles, and at the ZrN/Al matrix interface porosity was observed [7].

The results of the microstructural characterization of R9R010 can be used to help explain some of the observed behavior for the EFUTURE samples. At a fission density of around 5.2×10^{21} f/cm^3, fission gas bubbles in irradiated U-7Mo particles can become interconnected in such a way as to provide pathways to the U-7Mo/matrix interface. These pathways likely allow for a

some fraction of the fission gas to escape the fuel particle and migrate to the interface, along with solid fission products. The interaction layers that are present at the interface are amorphous and do not retain the fission gas effectively (i.e, the fission gases are mobile). As the fission gases are transported to the U-7Mo/interaction layer interface, fission gas bubbles can grow and can become interconnected in the layers and at the IL/matrix interfaces, and eventual fuel plate blistering can occur. Another result of the creation of pathways in the irradiated U-7Mo to the U-7Mo/matrix interface is the creation of short-circuit diffusion paths for the fast diffusion of Al into the fuel particles, and a U-Al interaction product can develop that penetrates into the U-7Mo. For Mg-matrix dispersion fuel, the phenomena observed for EFUTURE does not transpire. The Mg-matrix dispersion fuel contains only crystalline phases in the fuel meat. Therefore, when pathways are created to the Mg matrix interface, the fission gas that can escape the fuel particle does not enter an amorphous interaction layer (since none exists), but instead it comes into contact with a relatively robust, crystalline Mg matrix. The result is not the formation of large, interconnecting fission gas bubbles, but instead an overall fuel meat microstructure that displays little change in morphology. Also, even though pathways become available for fast diffusion of the matrix material into the U-7Mo, U and Mg are immiscible and so Mg diffusion does not take place.

For the SELENIUM fuel plates, the penetration of Al into the U-7Mo at fission densities near 5.2 x 10^{21} f/cm^3 will be tied to the behavior of the ZrN coating (presence of cracks, imperfections, etc.). The migration of the fission gases from the fuel particles, through the ZrN, and to the ZrN/matrix interface will also likely be tied to the microstructure of the ZrN, and when the fission gas can migrate through the ZrN, pores can be created at the ZrN/matrix interface.

4.2 Comparison to lower fission rate samples

In order to investigate the effects of fission rate on the microstructural evolution of U-7Mo during irradiation, the microstructure of R9R010 samples can be compared to microstructures observed for fuel plates irradiated to a similar fission density, but at a lower fission rate. Table 2 lists the irradiation conditions for R2R040, R3R050, and R0R010 high-flux samples irradiated in the RERTR-7 experiment, which are samples that meet these requirements, and have been characterized using SEM and FIB. Figure 19 shows the microstructures observed for characterized samples, along with the microstructure for a R9R010 sample. For samples with Al or Al-Si matrix, one has to avoid the interaction layers that are present in the irradiated samples in order to effectively characterize the microstructure of irradiated U-7Mo. For Mg matrix fuel, no such interaction layer has to be avoided.
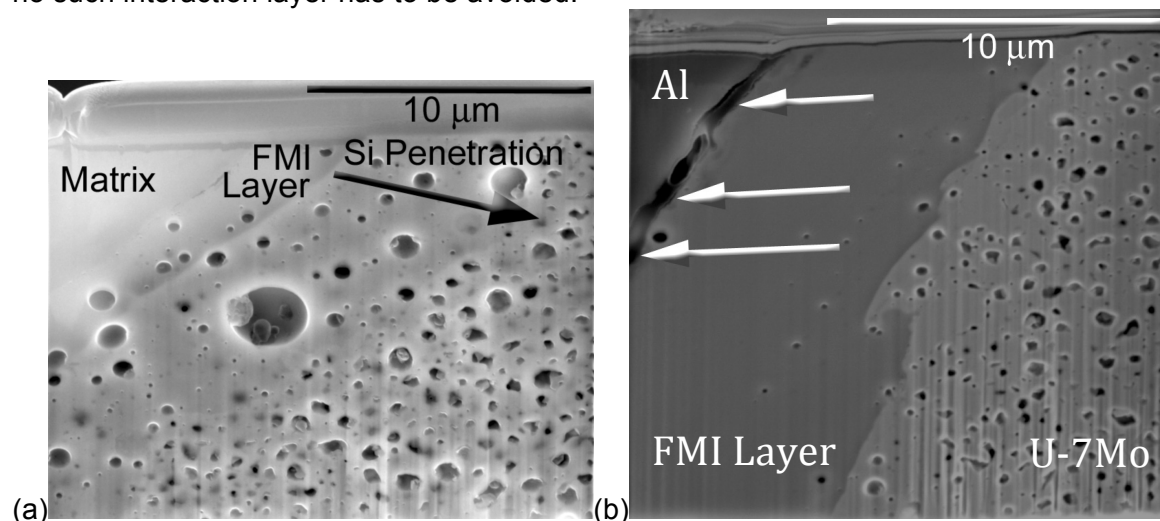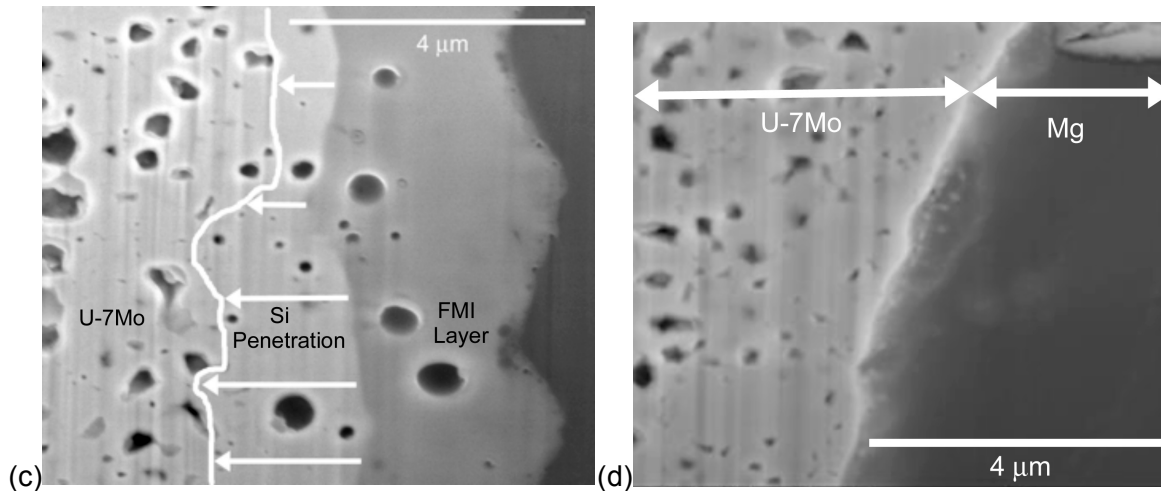
Fig. 19. Representative SEM micrographs of the microstructure observed for high-flux FIB samples taken from (a) R3R050 (AA4043 matrix), (b) R0R010 (Al matrix), (c) R2R040 (Al-2Si matrix), and (d) the high-flux R9R010 (Mg matrix) sample. The interaction layer present in the (a-c) images can complicate characterization of the irradiated U-7Mo microstructure.The arrows in (a) and (c) show how far Si has penetrated into the U-7Mo from the fuel/matrix interaction (FMI) layer. The arrows in (b) show where fission gas is enriched and porosity has developed at the FMI layer/Al interface. (d) shows that no FMI layer has formed between U-7Mo and Mg.

As shown in Fig. 11, some samples exhibit fairly obvious microstructural pathways to the U-7Mo/Mg interface. To date, the pathways observed in Fig. 11 have not been observed in the samples irradiated to similar fission density as R9R010, but at a lower fission rate. More samples from the lower fission rate plates should be characterized to get a better handle on whether or not these samples may actually have microstructural pathways that just have not identified yet. Based on the data currently available, the combination of high temperature, high power, and high fission rate may affect the microstructural response of U-7Mo such that fission gas bubbles are more prone to interconnection. As mentioned earlier, this could be due to a higher mobility of the fission gases due to higher temperatures and additional irradiation-generated defects present in higher fission rate samples. More mobility in the system can lead to increased interconnection of fission gas bubbles. It is plausible that such interconnection can lead to the release of fission gas from the fuel particles. At a finer scale (see Fig. 12), other pathways have been identified that are available for fission gas release. The irradiated U-7Mo grains for R9R010 are on the order of hundreds of nanometers in size and in most cases the larger gas bubbles have grain boundaries running into them. This means that a network of grain boundaries and large fission gas bubbles is available throughout the microstructure for migration of fission gas out of the fuel. Additional FIB samples will need to be analyzed from U-7Mo fuel samples irradiated under different combination of temperature, power, fission density, and fission rate to better determine how irradiation conditions affect the development of microstructures like those observed for the R9R010 sample.

Overall, the results in this paper show that there appear to be differences in the microstructure for the R9R010 plate compared to those irradiated in RERTR-7 at lower power, temperature, and fission rate. This suggests that the microstructural response of U-7Mo can be impacted by the reactor conditions employed during irradiation.

5.   Future Work

3D reconstruction has proven to be a critical characterization technique for studying porosity interconnection in irradiated samples, and it will be performed on more samples from R9R010 and fuel plates irradiated at lower fission rate to further investigate the effects of irradiation conditions on the interconnection of porosity. In addition, it would be beneficial for samples from SELENIUM to be characterized using FIB/SEM/TEM analysis and 3D reconstruction so that a direct comparison can be made to what has been observed for the R9R010 sample, and to investigate the performance of Si and ZrN coatings. This would provide confirmation that temperature, fission rate, and power impact the microstructural response of U-7Mo and coatings during irradiation. Irradiated dispersion samples with U-10Mo fuel particles will be characterized using FIB/SEM/TEM analysis and 3D reconstruction to see if increased Mo content in the fuel particles delays grain refinement and formation of the "high-burnup" microstructure at a particular set of irradiation conditions.

6.   Conclusions

Based on the SEM and TEM characterization of the microstructure of a low and high-flux sample taken from one of the most aggressively-irradiated U-7Mo dispersion fuel plates ever irradiated in ATR (R9R010), which was a fuel plate with U-7Mo particles and Mg matrix irradiated at high power, high temperature, and high fission rate, the following conclusions can be drawn:

1.   The phases (U-7Mo, Mg, and cladding) in U-7Mo dispersion fuel with Mg matrix remain crystalline during irradiation to high fission density, and negligible interaction occurs between the U-7Mo and Mg. As a result there is negligible indication of gross microstructural precursors (e.g., large pores from fuel particle to fuel particle through the Mg matrix) that might lead to fuel plate failure.

2. A U-7Mo fuel particle after irradiation to high fission density at high temperature, power, and fission rate contains interconnected porosity that can manifest itself as pathways for the possible transport of fission gases and/or solid fission products to the U-7Mo/matrix interface. Since there are no signs of large pores at the U-7Mo/Mg interface, this interface appears to remain robust even though there may be significant fission gas pressure at different fuel meat locations during irradiation.

3. Based on the comparisons of the R9R010 microstructure with those for samples irradiated to a very similar fisison density, but at lower temperatures, power, and fission rate, the response of U-7Mo to irradiation may be affected by the aggressive irradiation conditions, in terms of the amount of fission gas bubbles that become interconnected, the extent that fission products are transported through the microstructure, and the extent that a matrix material like Al may penetrate into the U-7Mo along microstructural pathways. More sample characterization will be required to definitively confirm the effect of the combination of high fission rate, high temperature, and high power on the microstructural evolution of U-7Mo fuel particles.

References

[1]. M. K. Meyer et al, Nucl. Energy and Tech. 46(2) (2014) 169-182.
[2]. S. Van den Berghe et al., J. Nucl. Mater. 442 (2013) 60-68.
[3]. D. D. Keiser, Jr. et al., RRFM 2012, Prague, Czech Republic, March 18-22, 2012.
[4]. Dennis D. Keiser, Jr. et al., Nucl. Energy and Tech. 46(2) (2014) 147-158.
[5]. Y. Zhong et al., CALPHAD: Comput. Coupling Phase Diagrams Thermochem. 29 (2005) 303-311.
[6]. J. Gan et al., J. Nucl. Mater. 424 (2012) 43-50.
[7]. Ann Leenaers, "Surface-engineered low-enriched Uranium-Molybdenum fuel for research reactors," Ph. D. Thesis, University of Gent (2014).
[8]. A. Leenaers et al., J. Nucl. Mater. 441 (2013) 439-448.